Title

Quantifying sources and sinks of reactive gases in the lower atmosphere using airborne flux observations

Journal

Geophysical Research Letters, 42(19)

ISSN

0094-8276

Authors

Wolfe, GM
Hanisco, TF
Arkinson, HL
et al.

Publication Date

2015-10-16

DOI

10.1002/2015gl065839

AGU PUBLICATIONS

Geophysical Research Letters

RESEARCH LETTER
10.1002/2015GL065839

Key Points:
- Airborne flux observations for a suite of reactive gases
- Direct constraints on production, loss, and surface-atmosphere exchange
- Comprehensive evaluation of chemical budgets over a temperate forest

Supporting Information:
- Texts S1–S8, Figures S1–S22, and Tables S1–S6

Correspondence to:
G. M. Wolfe,
glenn.m.wolfe@nasa.gov

Citation:
Wolfe, G. M., et al. (2015), Quantifying sources and sinks of reactive gases in the lower atmosphere using airborne flux observations, *Geophys. Res. Lett.*, *42*, 8231–8240, doi:10.1002/2015GL065839.

Received 18 AUG 2015
Accepted 23 SEP 2015
Accepted article online 28 SEP 2015
Published online 10 OCT 2015

Quantifying sources and sinks of reactive gases in the lower atmosphere using airborne flux observations

G. M. Wolfe[1,2], T. F. Hanisco[1], H. L. Arkinson[3], T. P. Bui[4], J. D. Crounse[5], J. Dean-Day[4,6], A. Goldstein[7], A. Guenther[8], S. R. Hall[9], G. Huey[10], D. J. Jacob[11,12], T. Karl[13], P. S. Kim[11], X. Liu[10], M. R. Marvin[3,14], T. Mikoviny[15], P. K. Misztal[7], T. B. Nguyen[5], J. Peischl[16,17], I. Pollack[16,17], T. Ryerson[16], J. M. St. Clair[5], A. Teng[5], K. R. Travis[11], K. Ullmann[9], P. O. Wennberg[5,18], and A. Wisthaler[15,19]

[1]Atmospheric Chemistry and Dynamics Laboratory, NASA Goddard Space Flight Center, Greenbelt, Maryland, USA, [2]Joint Center for Earth Systems Technology, University of Maryland Baltimore County, Baltimore, Maryland, USA, [3]Department of Oceanic and Atmospheric Science, University of Maryland, College Park, Maryland, USA, [4]Atmospheric Chemistry and Dynamics Branch, NASA Ames Research Center, Moffett Field, California, USA, [5]Division of Geological and Planetary Sciences, California Institute of Technology, Pasadena, California, USA, [6]Bay Area Environmental Research Institute, Petaluma, California, USA, [7]Department of Environmental Science, Policy and Management, University of California, Berkeley, California, USA, [8]Atmospheric Sciences and Global Change Division, Pacific Northwest National Laboratory, Richland, Washington, USA, [9]Atmospheric Chemistry Division, National Center for Atmospheric Research, Boulder, Colorado, USA, [10]School of Earth and Atmospheric Sciences, Georgia Institute of Technology, Atlanta, Georgia, USA, [11]Department of Earth and Planetary Sciences, Harvard University, Cambridge, Massachusetts, USA, [12]School of Engineering and Applied Sciences, Harvard University, Cambridge, Massachusetts, USA, [13]Institute for Meteorology and Geophysics, University of Innsbruck, Innsbruck, Austria, [14]Department of Chemistry, University of Maryland, College Park, Maryland, USA, [15]Department of Chemistry, University of Oslo, Oslo, Norway, [16]Chemical Sciences Division, NOAA Earth System Research Laboratory, Boulder, Colorado, USA, [17]Cooperative Institute for Research in Environmental Sciences, University of Colorado Boulder, Boulder, Colorado, USA, [18]Division of Engineering and Applied Science, California Institute of Technology, Pasadena, California, USA, [19]Institute of Ion Physics and Applied Physics, University of Innsbruck, Innsbruck, Austria

Abstract Atmospheric composition is governed by the interplay of emissions, chemistry, deposition, and transport. Substantial questions surround each of these processes, especially in forested environments with strong biogenic emissions. Utilizing aircraft observations acquired over a forest in the southeast U.S., we calculate eddy covariance fluxes for a suite of reactive gases and apply the synergistic information derived from this analysis to quantify emission and deposition fluxes, oxidant concentrations, aerosol uptake coefficients, and other key parameters. Evaluation of results against state-of-the-science models and parameterizations provides insight into our current understanding of this system and frames future observational priorities. As a near-direct measurement of fundamental process rates, airborne fluxes offer a new tool to improve biogenic and anthropogenic emissions inventories, photochemical mechanisms, and deposition parameterizations.

1. Introduction

The convective boundary layer (CBL) is the rapidly mixed lowest 1–2 km of the troposphere in direct contact with Earth's surface. Chemical and physical processes within the CBL shape the composition of the lower atmosphere and its relationship with other Earth systems. Emissions of reactive gases, including volatile organic compounds (VOC) and nitrogen oxides ($NO_x = NO + NO_2$), originate from natural and anthropogenic sources at the surface. Photochemistry transforms these gases into secondary products like ozone (O_3) and organic aerosol, impacting global air quality and climate [*Fiore et al.*, 2012]. Dry deposition removes atmospheric pollutants and supplies nitrogen and reactive oxygen to vegetation. Turbulent mixing governs the evolution of CBL structure and entrainment of overlying air masses [*de Arellano et al.*, 2011]. Our ability to predict the state of the lower atmosphere hinges on our comprehension of these processes.

The interplay of biology, meteorology, chemistry, and surface interactions makes the biosphere-atmosphere interface a particularly complex region of the CBL (Figure 1). Forests emit copious VOC including isoprene, a conjugated diene that comprises one third of total global VOC emissions [*Guenther et al.*, 2012]. Oxidation of

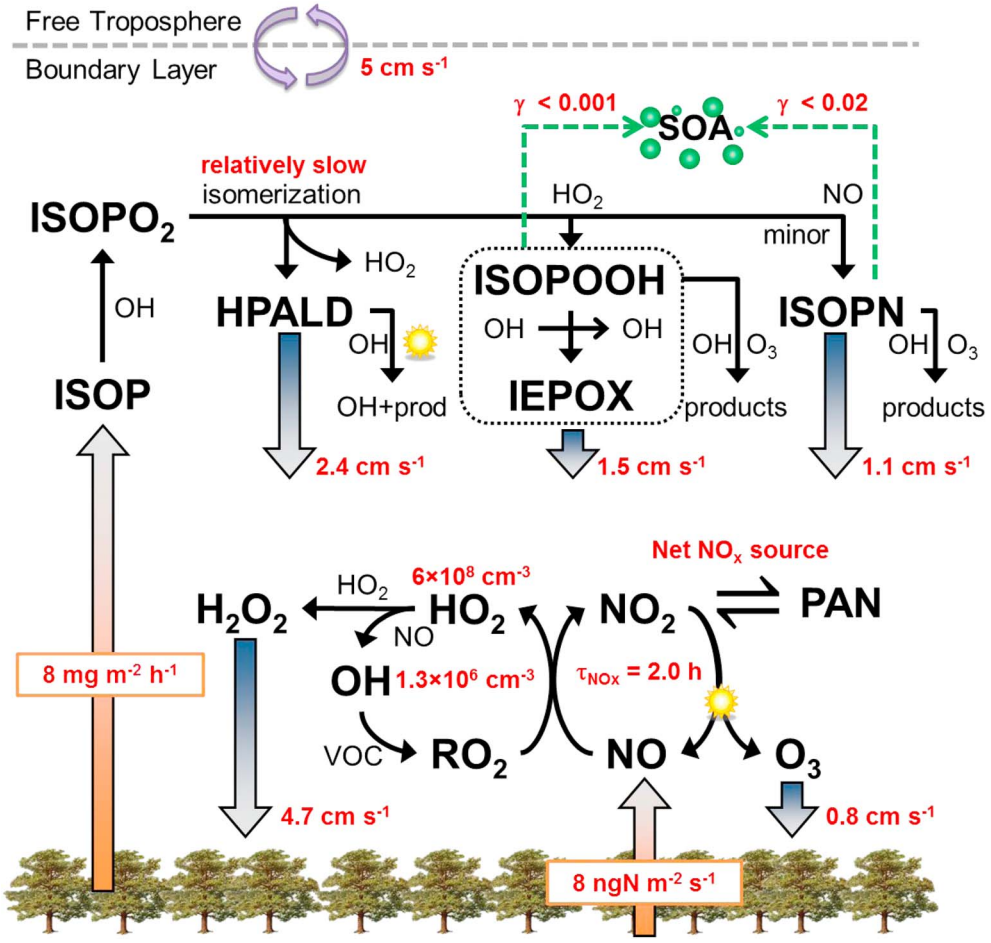

Figure 1. Key processes in the forested daytime CBL. Red text highlights parameters quantified via flux analysis. Orange arrows denote emission, blue arrows denote deposition, and green dashed arrows denote heterogeneous uptake. Only reactions central to the discussion are shown.

isoprene by hydroxyl radical (OH) generates myriad oxygenated VOC (oVOC) that may undergo further reaction, deposit to forest surfaces or partition to secondary organic aerosol (SOA) [*Goldstein and Galbally*, 2007]. This chemistry also fuels ozone production in the presence of NO_x, which is emitted via combustion and soil microbial processes. Termination of radical cycling produces compounds like hydrogen peroxide (H_2O_2) and nitric acid (HNO_3), which are lost via dry deposition or rainout and may foster feedbacks through impacts on carbon and nitrogen cycles [*Magnani et al.*, 2007].

While our understanding of this system is evolving rapidly, considerable uncertainties persist. Isoprene emission inventories can differ by factors of 2 or more [*Hogrefe et al.*, 2011; *Warneke et al.*, 2010]. Newly discovered isoprene degradation products can be potent radical and aerosol precursors [*Paulot et al.*, 2009; *Peeters et al.*, 2009], yet models still struggle to explain observed radical concentrations [*Stone et al.*, 2012] and SOA mass [*Heald et al.*, 2011]. Most oVOC likely undergo deposition or bidirectional exchange [*Nguyen et al.*, 2015; *Park et al.*, 2013], but measurements are too sparse to adequately constrain these processes. Even in the case of ozone, for which field observations are plentiful, deposition fluxes over forests can vary from model to model by factors of 3 or more [*Hardacre et al.*, 2014].

We present a unique data set that combines the payload and spatial coverage of a flying laboratory with the strengths of eddy covariance (EC) to constrain fundamental CBL processes. The EC technique affords a direct measure of vertical fluxes, which are sensitive to both surface and in situ processes. Previous work, for example, has applied airborne EC methodology to study ozone [*Lenschow et al.*, 1981] and isoprene [*Karl et al.*, 2013; *Misztal et al.*, 2014]. Figure 1 summarizes key parameters derived in our analysis. The

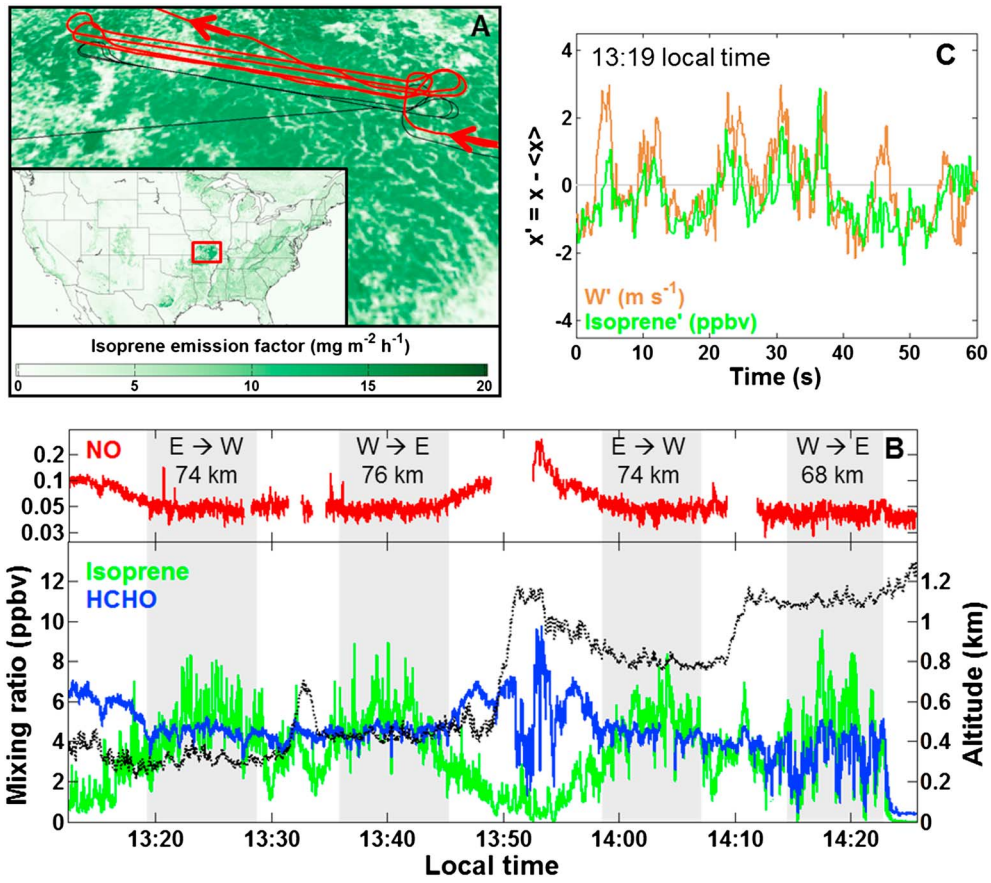

Figure 2. (a) Map of the study area and flight pattern (red line: flight track and black line: ground track). Green shading corresponds to isoprene emission factors from the latest version of MEGAN [*Guenther et al.*, 2012]. The inset shows emission factors for the whole U.S. with a red box indicating the Ozarks. (b) Observed 1 Hz mixing ratios of isoprene, formaldehyde (HCHO) and NO, along with aircraft altitude (broken line) relative to ground level. Shading highlights the data segments used in flux calculations. (c) Example correlation of isoprene and vertical wind speed for a portion of the first flight leg. W′ and isoprene′ represent the instantaneous deviation from the whole flight leg mean and 20 s running mean, respectively.

synergistic information obtained from simultaneous fluxes of multiple reactive species provides a self-consistent picture of the CBL and a benchmark for testing our understanding of isoprene-oxidant chemistry and biosphere-atmosphere interactions.

2. Mission and Methods

We utilize measurements collected on 6 September 2013 over the Ozark Mountains during the NASA SEAC^{4}RS (Studies of Emissions and Atmospheric Composition, Clouds and Climate Coupling by Regional Surveys) mission. Figure 2a maps the flight track together with isoprene emission factors from MEGAN (Model of Emissions of Gases and Aerosols from Nature) [*Guenther et al.*, 2012]. Colloquially known as the "isoprene volcano" [*Wiedinmyer et al.*, 2005], this region is a dense oak forest with sparse local anthropogenic emissions. The NASA DC-8 entered from the east at 13:10 local time and executed a series of four vertically stacked 75 km long transects in the CBL. Weather was mostly sunny and warm (potential temperature = 302 K) with uniform horizontal winds from S-SE at 3 m s^{-1} and a strong subsidence inversion at z_i = 1060 m. These conditions are near ideal for evaluating turbulent fluxes.

Observations of isoprene, formaldehyde, and nitric oxide (NO) reveal two distinct chemical regimes during this flight (Figure 2b). Elevated NO on the eastern end indicates a pollution plume, likely transported from an upwind power plant. Enhanced NO_x accelerates the radical turnover rate in this air mass, converting isoprene to formaldehyde and other products. In the middle and western portions, NO mixing ratios of 0.05 ppbv are more typical of the continental background, while isoprene is elevated due to both strong

emissions and slower oxidation. Our analysis will focus on the latter region, indicated by the shaded segments in Figure 2b. Section S1, Figures S1–S4, and Table S1 in the supporting information provide further details on the flight location and measurements.

The high variability of isoprene in the CBL illustrates the interplay of chemistry and turbulence. Isoprene is emitted at the surface and transported vertically via turbulent eddies, while OH and ozone destroy isoprene as it mixes. Thus, upward moving eddies are enriched in isoprene compared to downward moving eddies (Figure 2c). This concept forms the core of our methodology: by exploiting the natural variability created by turbulent mixing, we can extract quantitative information on both surface-atmosphere exchange and in situ chemical transformations.

For each of the four flight segments, we calculate EC fluxes of isoprene, hydrogen peroxide (H_2O_2), ozone (O_3), NO_x, peroxyacetyl nitrate (PAN), several isoprene oxidation products, and sensible heat. In addition to traditional EC, we also apply wavelet transforms to obtain horizontally resolved surface fluxes [*Misztal et al*., 2014]. Details on flux calculations, including spectral and error analysis, are available in Text S2. The flux footprint half-widths for legs 1 to 4 are 0.6, 1.0, 1.4, and 2.1 km, increasing with height (Text S2). Where possible, surface fluxes are compared to output from a $25 \times 25\ km^2$ GEOS-Chem 3-D global chemical transport model simulation [*Wang et al*., 1998]. Derived radical concentrations (section 3.4) are compared to both GEOS-Chem and a 0-D box model simulation incorporating the Master Chemical Mechanism (MCMv3.2) [*Jenkin et al*., 1997; *Saunders et al*., 2003]. Both models are described in Text S7.

To interpret vertical flux profiles (Figures 3 and 4), we apply the scalar budget equation,

$$\frac{\partial C}{\partial t} = Q - A - \frac{\partial F}{\partial z} \tag{1}$$

which states that the time rate of change in concentration of a scalar, C, is the sum of rates of in situ production and loss (Q), horizontal advection (A, also known as horizontal flux divergence), and vertical flux divergence. Rearranging, integrating over altitude (z) and assuming all terms are approximately constant for a well-mixed CBL over the ~1 h flight pattern yields a simplified description of the flux profile:

$$F(z) = \left(Q - A - \frac{\partial C}{\partial t}\right)_{avg} z + F_0 \tag{2}$$

The intercept (F_0) reflects surface exchange (emission or deposition), while the slope contains the combined effects of chemistry, advection, and storage (the vertical integral of $\partial C/\partial t$). The latter two terms are estimated from concentration data along the transects (Text S3), and the chemical term is calculated as the residual sum of flux divergence, advection, and storage (Table S2). For species where Q varies strongly with altitude (e.g., Figures 4a and 4b), this linear relationship can be replaced with a more rigorous treatment of vertically varying process rates (Text S4). All quoted uncertainties represent 95% confidence intervals propagated from error-weighted least squares fits to flux profiles.

3. Results and Discussion

3.1. Isoprene Emissions

Despite decades of research spanning leaf level to continental scales, accurate parameterization of biogenic VOC emissions remains challenging. Previous observations of in situ isoprene concentrations [*Carlton and Baker*, 2011] and satellite-derived formaldehyde columns [*Millet et al*., 2008] indicate that MEGAN overestimates isoprene emissions by 30 to 50% over the Ozarks. Extrapolation of the isoprene flux profile (Figure 3a) yields a surface flux of $8 \pm 1\ mg\ m^{-2}\ h^{-1}$, 40% lower than the mean value of $14\ mg\ m^{-2}\ h^{-1}$ calculated within GEOS-Chem using MEGAN. Wavelet analysis (Figure 3b) illustrates that local emissions vary by more than a factor of 2 over the transect and that the greatest model-measurement disagreement occurs at the eastern end, near the heart of the Ozarks (Figure S20). Work is currently underway to apply airborne fluxes to a broader evaluation of MEGAN in other regions [*Karl et al*., 2013; *Misztal et al*., 2014]. Such measurements will be invaluable for interpretation of future high-resolution satellite observations, linking global-scale continuous emission estimates and ecosystem-level responses.

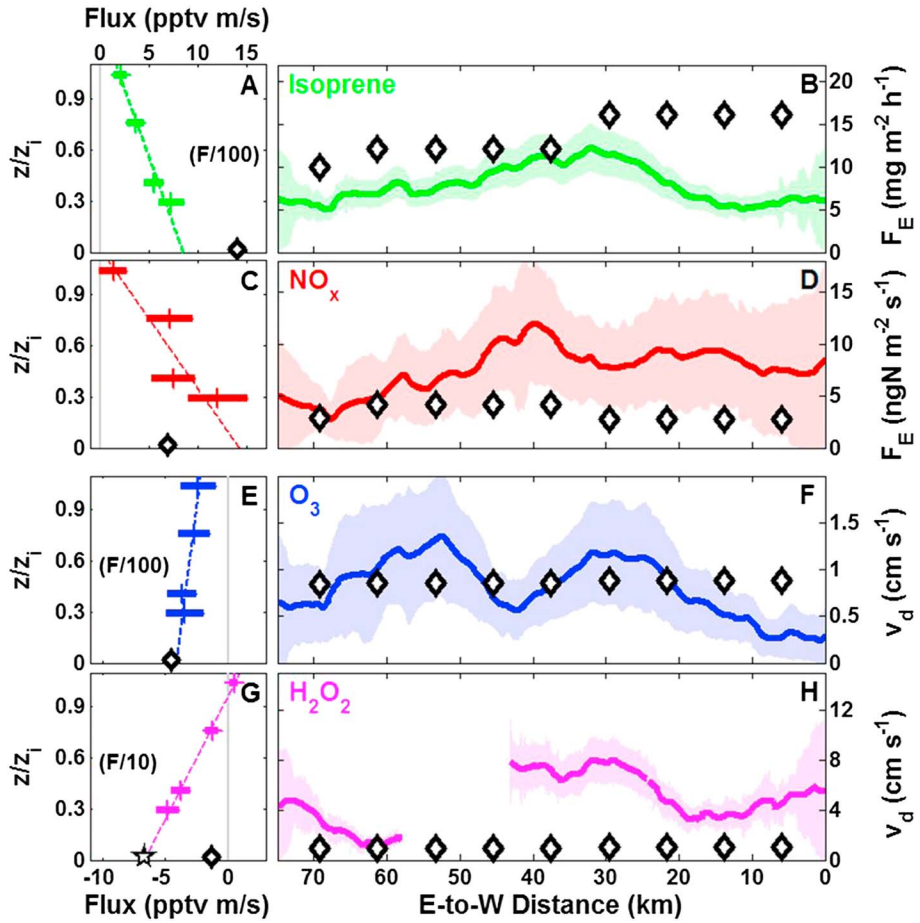

Figure 3. (a, c, e, and g) Vertical flux profiles for isoprene, NO_x, ozone, and H_2O_2. The top scale corresponds to the upper two plots, and the bottom scale to the lower two. Scaling factors are indicated in parentheses (for left plots only). Altitude is normalized to the CBL height (z_i = 1060 m). Crosses and bars represent observed fluxes and 95% confidence intervals. Dashed lines are linear least squares fits. The star in Figure 3g is the theoretical H_2O_2 flux assuming no surface resistance (Text S6). Diamonds represent average surface fluxes from a GEOS-Chem simulation along the flight track. (b, d, f, and h) Horizontal profiles of surface fluxes. Solid lines and shaded areas represent observed fluxes and 95% confidence intervals derived from wavelet transforms along the first transect, corrected to an assumed canopy height of 20 m using observed flux divergence and smoothed with a 10 km running mean (section S2.4 in Text S2). Emission fluxes (F_E) and deposition velocities (v_d) are given in traditional units. Diamonds represent GEOS-Chem results.

3.2. Emissions and Fate of NO_x

Soils emit 15% of global NO_x and are a primary source of reactive nitrogen in many rural areas [*Jaeglé et al.*, 2005]. Airborne fluxes can provide a direct constraint on NO_x emissions at an aggregated scale appropriate for comparison to models and satellite observations. It is most appropriate to consider the total NO_x flux (Figure 3c), as NO and NO_2 interconvert rapidly. The extrapolated surface NO_x emission of 8 $\pm$ 3 g N m^{-2} s^{-1} is substantially higher than the GEOS-Chem flux of 4 ng N m^{-2} s^{-1}, which represents the net flux of NO from soils (75%), fertilizer (14%), and anthropogenic sources (18%) less NO_2 deposition (−7%). Modeled NO_x emissions agree reasonably well with observations in the west but are substantially lower in the east (Figure 3d). Model-measurement differences may stem from soil heterogeneity or environmental response functions (e.g., temperature and soil moisture). Accurate representation of soil NO_x emissions is crucial for modeling atmospheric chemistry in pristine forests (e.g., the Amazon) and will be increasingly important in the U.S. as anthropogenic NO_x emissions continue to decline.

Conversion to higher oxides of nitrogen governs the lifetime of NO_x and thus the spatial extent of emission impacts. The combination of flux divergence and storage (Table S2) implies a net chemical

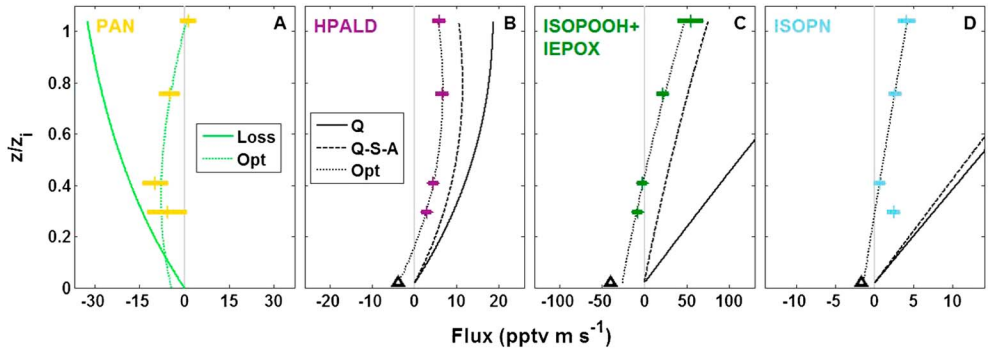

Figure 4. Vertical flux profiles of PAN and isoprene oxidation products. Crosses and bars represent calculated fluxes and 95% confidence intervals. (a) The solid green line is the predicted PAN flux from thermal loss only, while the dotted green line is the "optimized" flux including storage, advection, and primary PA production (section S4.5 in Text S4). (b–d) Solid lines are the "chemical flux" profiles predicted from consideration of gas-phase chemistry (section S4.6 in Text S4). Dashed lines are the sum of chemical, storage, and advection fluxes. Dotted lines are optimized profiles that include the above three terms plus surface deposition and missing production/loss rates (section S4.6 in Text S4). Triangles represent top-of-canopy fluxes calculated from daytime average deposition velocities for a similar forest [*Nguyen et al.*, 2015].

lifetime of 2.0 ± 0.5 h. For comparison, the NO_x lifetime estimated from consideration of formation of nitric acid, alkyl nitrates (ANs), and peroxyacetyl nitrate (PAN) is 1.4 ± 0.4 h (section S4.4 in Text S4). This difference implies an additional in situ NO_x source. Formation ANs comprises >90% of calculated gross NO_x loss, but subsequent processing of these compounds may release some NO_x. Ascribing the entire difference between observed and calculated NO_x lifetimes to such a mechanism yields a bulk AN recycling efficiency (NO_x produced per NO consumed) of 29 ± 29%, bracketing the range of previous estimates for isoprene-rich environments [*Horowitz et al.*, 2007; *Perring et al.*, 2009]. Our results indicate that NO_x recycling via isoprene-derived ANs is nonnegligible and may be an important NO_x source in remote regions [*Paulot et al.*, 2012].

PAN, which exists in thermal equilibrium with its precursors (peroxyacetyl radical (PA) and NO_2), can be a source or sink of NO_x. Fluxes of PAN are sensitive to temperature [*Wolfe et al.*, 2009], resulting in vertical curvature as loss decreases with altitude (Figure 4a). Analysis of PAN fluxes (section S4.5 in Text S4 and Figure S21) reveals that PAN is a net source of NO_x in this case, with a CBL-average production rate of 0.006 ± 0.003 pptv s^{-1}. For comparison, the soil NO_x source is equivalent to 0.013 ± 0.005 pptv s^{-1} when distributed over the CBL. Thus, transport and decomposition of PAN may account for ~30% of total NO_x production in this region. In the supporting information, we further demonstrate that PAN fluxes can provide a top-down constraint on PA production, which is relevant to both the fate of NO_x and overall VOC oxidation [*LaFranchi et al.*, 2009].

3.3. Deposition of Ozone, H_2O_2, and oVOC

Dry deposition—the uptake of gases by terrestrial surfaces—is typically described by a deposition velocity, v_d, which intrinsically depends on turbulence, gas, and surface properties. Variants of the resistance framework of *Wesely* [1989] are widely used to calculate v_d, but observational constraints for these parameterizations are often limited. Extrapolation of airborne fluxes to the surface provides a direct measure of v_d for several species.

Despite a substantial body of laboratory and field work on ozone deposition, global models may overpredict or underpredict measured ozone fluxes by as much as a factor of 2 [*Hardacre et al.*, 2014]. We derive an ozone v_d of 0.8 ± 0.1 cm s^{-1} over the Ozarks, in agreement with the mean GEOS-Chem value of 0.9 cm s^{-1} (Figure 3e). The structure of wavelet fluxes (Figure 3f) reflects a combination of surface heterogeneity and varying chemical conditions. For example, the local minimum near the middle of the transect (Figure 3f) is coincident with the maximum NO_x flux (Figure 3d) and an invariant H_2O_2 deposition velocity (Figure 3h), consistent with enhanced ozone production at this location. This behavior underscores the value of a comprehensive payload and the need to exercise caution when interpreting reactive gas fluxes.

H_2O_2 is an important participant in aqueous-phase chemistry [*Ervens et al.*, 2014] and can be a major precursor of plant-damaging reactive oxygen species [*Nguyen et al.*, 2015]. The measured H_2O_2 v_d of 4.7 ± 0.4 cm s^{-1} is significantly faster than the model prediction of 1.0 cm s^{-1} (Figure 3g) but close to the value calculated for a negligible surface resistance (4.6 ± 0.4 cm s^{-1}). Variability in wavelet-derived v_d (Figure 3h) roughly tracks underlying leaf area on the western end but not the east (Figure S2), possibly implying changes in other surface characteristics or in the (assumed constant) chemical flux divergence. Despite long-recognized problems with peroxide deposition [*Ganzeveld et al.*, 2006; *Hall et al.*, 1999; *Nguyen et al.*, 2015], models continue to use flawed parameterizations. GEOS-Chem overpredicts H_2O_2 concentrations by 60% for this case, likely because H_2O_2 losses are underestimated. We calculate that deposition comprises 83% of total H_2O_2 loss in this environment.

Figures 4b–4d present fluxes for three major isoprene-derived oVOC : hydroperoxyaldeydes (HPALD), the sum of isoprene hydroxyhydroperoxides (ISOPOOH) and isoprene dihydroxyepoxides (IEPOX), and isoprene hydroxynitrates (ISOPN). Each class of compounds represents a distinct oxidation pathway (Figure 1). Deposition velocities (Figure 1 and Table S5), derived from a rigorous treatment of chemical flux divergence (section S4.6 in Text S4), are comparable to those obtained from tower-based observations over another mixed forest in the southeast U.S. [*Nguyen et al.*, 2015]. Deposition lifetimes range from 12 to 26 h (Table S5), challenging the common practice of assigning a single "physical loss lifetime" to all such species in 0-D box models [*Edwards et al.*, 2013]. oVOC deposition can be a major sink for SOA precursors [*Knote et al.*, 2015] and is a conduit for atmosphere-biosphere transfer of carbon, nitrogen, and reactive oxygen [*Nguyen et al.*, 2015; *Park et al.*, 2013]. A concerted effort is needed to retool deposition parameterizations for more accurate representations of physicochemical driving processes.

3.4. Radical Concentrations and Recycling

For species where the chemical term dominates the budget equation, flux divergence affords a near-direct measure of reaction rates. *Karl et al.* [2013] demonstrated that negative isoprene flux divergence (Figure 3a) reflects loss via reaction with OH. Likewise, positive H_2O_2 flux divergence (Figure 3g) signifies production via self-reaction of hydroperoxyl (HO_2) radicals. Using these relationships (sections S4.1 and S4.2 in Text S4), we derive observationally constrained average concentrations of OH ($(1.3 \pm 0.3) \times 10^6$ cm^{-3}) and HO_2 ($(6 \pm 1) \times 10^8$ cm^{-3}). It is also theoretically possible to quantify total peroxyl radicals (HO_2 and RO_2) from ozone flux divergence, but overwhelming contributions from storage and advection confound this calculation in the present case (section S4.3 in Text S4).

Models routinely underpredict radical concentrations in high-isoprene, low-NO_x regions, but the extent to which this implies problems with measurements or mechanisms remains debated [*Mao et al.*, 2012; *Rohrer et al.*, 2014]. Comparison of flux-derived radical concentrations with GEOS-Chem and a measurement-constrained 0-D box model (Table S6) shows good agreement for HO_2, while OH is underpredicted by 75% and 30%, respectively. Greater underprediction of GEOS-Chem may be partly explained by overestimated isoprene emissions as discussed above. The discrepancy with the box model is comparable to the typical uncertainty of direct OH measurements and smaller than some previously reported model-measurement differences in similar regions [*Stone et al.*, 2012]. Sensitivity simulations performed with the box model reveal that adoption of the latest theoretical HPALD production rate [*Peeters et al.*, 2014] has no impact on model OH (Table S6). Reducing the isoprene + OH rate constant by 50% to mimic reactant segregation [*Krol et al.*, 2000] proportionally raises OH, but reduced radical production is inconsistent with oVOC fluxes (see below). Both modifications degrade HO_2 agreement. The SEAC^{4}RS payload did not include HO_x observations. Such a comparison on future missions would facilitate efforts to investigate measurement artifacts in biogenic-rich environments [*Fuchs et al.*, 2011; *Mao et al.*, 2012].

Isomerization of isoprene hydroxyalkylperoxyl radicals ($ISOPO_2$) has emerged as a promising solution for underprediction of HO_x in biogenic regions [*Peeters et al.*, 2009]. This mechanism efficiently recycles radicals and bypasses radical-terminating peroxide formation in low-NO_x conditions. Its impact hinges on the isomerization rate constant, for which the latest theoretical estimate exceeds the experimentally inferred value by a factor of 1.8 [*Crounse et al.*, 2011; *Peeters et al.*, 2014]. HPALDs are a unique and quantitative marker for this chemistry. The temperature dependence of isomerization, which slows by a factor of 2.2 between the ground and 1 km, manifests in the curvature of the HPALD flux profile (Figure 4b). Also shown in Figure 4b is the

theoretical flux profile obtained from consideration of vertically varying production and loss rates in analogy to equation (2) (section S4.6 in Text S4). With the experimental HPALD production rate [*Crounse et al*., 2011], we are able to close the HPALD flux budget. To our knowledge, this represents the first observationally constrained evaluation of this mechanism.

3.5. Aerosol Uptake

Isoprene oxidation products may comprise ~50% of global SOA [*Henze and Seinfeld*, 2006]. SOA growth is a complex, multiphase problem, but from the perspective of gas-phase precursors, it is a first-order loss. Flux divergence provides a direct constraint on the net chemical tendency of oVOC (section S4.6 in Text S4), which can be compared with theoretical predictions to quantify potential missing sources or sinks.

IEPOX can be a major contributor to SOA mass in regions with low-NO_x and high sulfate activity [*Xu et al*., 2015]. The theoretical chemical flux for ISOPOOH + IEPOX exhibits a strong positive slope (Figure 4c) due to fast production of ISOPOOH and slow gas-phase oxidation of IEPOX. Flux divergence is considerably more shallow, but most of this difference reflects a large positive storage term (Table S2). Thus, we can close the budget of ISOPOOH + IEPOX through consideration of gas-phase chemistry alone. These results support an upper limit IEPOX uptake coefficient (γ) of 0.001 ± 0.004, representing the probability that a gas molecule will be taken up upon contact with an aerosol surface. In contrast, a recently published parameterization [*Gaston et al*., 2014] gives a significantly faster γ of 0.04 ± 0.03. Other limiting factors may be at play here, such as suppression of uptake by organic coatings [*Gaston et al*., 2014] or phase separation [*Smith et al*., 2012]. Furthermore, the effective Henry's law coefficient for IEPOX is not well constrained. Using a lower value as recommended by *McNeill et al*. [2012] gives a parameterized γ of 0.010 ± 0.006.

ISOPN may also partition to aerosol, but considerably less attention has been devoted to this process. Observed ISOPN flux divergence is shallower than that predicted with gas-phase chemistry, even after including storage and advection (Figure 4d). This difference implies a significant missing ISOPN sink. Attributing the difference to aerosol uptake yields an upper limit γ of 0.02 ± 0.01. Recent lab work has revealed that hydrolysis rates vary by more than 2 orders of magnitude between ISOPN isomers [*Jacobs et al*., 2014]. Our results, which represent a weighted sum for all ISOPN isomers, indicate that heterogeneous loss may comprise 70% of the total ISOPN sink in this environment.

Flux observations provide a valuable constraint on gas-aerosol partitioning, but the subsequent fate of organics remains unclear. In particular, it is unknown what fraction of the organic carbon evaporates following heterogeneous processing. Simultaneous measurements of oVOC fluxes and aerosol composition will provide better closure of the reactive carbon budget and a more complete understanding of the isoprene-SOA system.

3.6. Entrainment

Fluxes of short-lived compounds like isoprene are well suited for quantifying the rate of mixing between the CBL and the overlying free troposphere (FT) [*Karl et al*., 2013]. The entrainment flux can be parameterized as $v_e \Delta C$, where v_e is an entrainment velocity and ΔC is the CBL-FT concentration difference. Effectively a measure of boundary layer growth, v_e will vary in both time and space. Isoprene is well suited for this calculation due to its large CBL-FT concentration gradient. Using observed isoprene fluxes and concentrations, we calculate $v_e = 5 \pm 1\ \mathrm{cm\ s^{-1}}$ for this well-developed CBL, within the range of values reported by *Karl et al*. [2013]. Figure S22 compares entrainment velocities calculated from other flux profiles; those that do not agree with the isoprene-derived v_e typically exhibit weak CBL-FT concentration gradients or significant storage terms. This parameter is rarely constrained by observations but can be crucial for representing the diurnal evolution of boundary layer composition [*de Arellano et al*., 2011].

4. Outlook

The ecosystem-level view inherent to airborne fluxes is ideal for refinement of model parameterizations and mechanisms. Future airborne missions could acquire fluxes over diverse surfaces (forest, farmland, ocean, urban and industrial areas, etc.) and under contrasting environmental conditions to build an extensive data set. Such measurements can be obtained in tandem to other mission objectives, adding value to a chemistry-oriented payload. The EC technique inherently requires turbulence and is thus best applied in unstable

daytime boundary layers. We stress that the synergistic information afforded by a broad instrument suite is crucial for developing a self-consistent picture of the CBL.

Airborne fluxes hold promise well beyond the cases presented here. For example, simultaneous measurements of speciated and total oxidized nitrogen (NO_y) would permit characterization of the NO_y flux budget and identification of unknown processes, such as nitrous acid production [*Li et al.*, 2014]. Other potential topics include the link between isoprene emissions and plant productivity [*Unger et al.*, 2013], bidirectional ocean exchange of small-chain oVOC [*Coburn et al.*, 2014], and aerosol chemistry and composition [*Farmer et al.*, 2013].

Acknowledgments

This work was supported by grants from the NASA ROSES SEAC4RS (NNH10ZDA001N and NNX12AC06G) and ACCDAM (NNX14AP48G and NNX14AP46G) programs. T.B.N. acknowledges support from NSF PRF award AGS-1331360. Isoprene measurements were supported by the Austrian Federal Ministry for Transport, Innovation and Technology (bmvit) through the Austrian Space Applications Programme (ASAP) of the Austrian Research Promotion Agency (FFG). A.W. and T.M. received support from the Visiting Scientist Program at the National Institute of Aerospace (NIA). We thank the DC-8 pilots, crew, payload operators, and mission scientists for their hard work and for the opportunity to calibrate the meteorological measurements. We are also grateful to NASA ESPO for mission logistics. We thank the Jimenez, Brock, and Anderson groups for use of aerosol data. We also thank L. Kaser, B. Yuan, S.-W. Kim, and J. Thornton for helpful discussions. All data used in this analysis are publicly available under the SEAC4RS DOI at 10.5067/Aircraft/SEAC4RS/Aerosol-TraceGas-Cloud.

The Editor thanks an anonymous reviewer for assisting in the evaluation of this paper.

References

Carlton, A., and K. Baker (2011), Photochemical modeling of the Ozark isoprene volcano: MEGAN, BEIS, and their impacts on air quality predictions, *Env. Sci. Technol.*, *45*(10), 4438–4445.

Coburn, S., I. Ortega, R. Thalman, B. Blomquist, C. W. Fairall, and R. Volkamer (2014), Measurements of diurnal variations and Eddy Covariance (EC) fluxes of glyoxal in the tropical marine boundary layer: Description of the Fast LED-CE-DOAS instrument, *Atmos. Meas. Tech.*, *7*, 3579–3595.

Crounse, J. D., F. Paulot, H. G. Kjaergaard, and P. O. Wennberg (2011), Peroxy radical isomerization in the oxidation of isoprene, *Phys. Chem. Chem. Phys.*, *13*(30), 13,607–13,613.

de Arellano, J. V. G., E. G. Patton, T. Karl, K. van den Dries, M. C. Barth, and J. J. Orlando (2011), The role of boundary layer dynamics on the diurnal evolution of isoprene and the hydroxyl radical over tropical forests, *J. Geophys. Res.*, *116*, D07304, doi:10.1029/2010JD014857.

Edwards, P. M., et al. (2013), OH reactivity in a South East Asian tropical rainforest during the Oxidant and Particle Photochemical Processes (OP3) project, *Atmos. Chem. Phys.*, *13*(18), 9497–9514.

Ervens, B., A. Sorooshian, Y. B. Lim, and B. J. Turpin (2014), Key parameters controlling OH-initiated formation of secondary organic aerosol in the aqueous phase (aqSOA), *J. Geophys. Res. Atmos.*, *119*, 3997–4016, doi:10.1002/2013JD021021.

Farmer, D. K., Q. Chen, J. R. Kimmel, K. S. Docherty, E. Nemitz, P. A. Artaxo, C. D. Cappa, S. T. Martin, and J. L. Jimenez (2013), Chemically resolved particle fluxes over tropical and temperate forests, *Aer. Sci. Technol.*, *47*(7), 818–830.

Fiore, A. M., et al. (2012), Global air quality and climate, *Chem. Soc. Rev.*, *41*(19), 6663–6683.

Fuchs, H., B. Bohn, A. Hofzumahaus, F. Holland, K. D. Lu, S. Nehr, F. Rohrer, and A. Wahner (2011), Detection of HO(2) by laser-induced fluorescence: Calibration and interferences from RO(2) radicals, *Atmos. Meas. Tech.*, *4*(6), 1209–1225.

Ganzeveld, L., J. Valverde-Canossa, G. K. Moortgat, and R. Steinbrecher (2006), Evaluation of peroxide exchanges over a coniferous forest un a single-column chemistry-climate model, *Atmos. Env.*, *40*, S68–S80.

Gaston, C. J., T. P. Riedel, Z. Zhang, A. Gold, J. D. Surratt, and J. A. Thornton (2014), Reactive uptake of an isoprene-derived epoxydiol to submicron aerosol particles, *Env. Sci. Technol.*, *48*, 11,178–11,186.

Goldstein, A., and I. Galbally (2007), Known and unexplored organic constituents in the Earth's atmosphere, *Env. Sci. Technol.*, *41*(5), 1514–1521.

Guenther, A. B., X. Jiang, C. L. Heald, T. Sakulyanontvittaya, T. Duhl, L. K. Emmons, and X. Wang (2012), The model of emissions of gases and aerosols from nature version 2.1 (MEGAN2.1): An extended and updated framework for modeling biogenic emissions, *Geosci. Mod. Dev.*, *5*, 1471–1492.

Hall, B., C. Claiborn, and D. Baldocchi (1999), Measurement and modeling of the dry deposition of peroxides, *Atmos. Env.*, *33*(4), 577–589.

Hardacre, C., O. Wild, and L. Emberson (2014), An evaluation of ozone dry deposition in global scale chemistry climate models, *Atmos. Chem. Phys.*, *15*, 6419–6436.

Heald, C. L., et al. (2011), Exploring the vertical profile of atmospheric organic aerosol: Comparing 17 aircraft field campaigns with a global model, *Atmos. Chem. Phys.*, *11*(24), 12,673–12,696.

Henze, D. K., and J. H. Seinfeld (2006), Global secondary organic aerosol from isoprene oxidation, *Geophys. Res. Lett.*, *33*, L09812, doi:10.1029/2006GL025976.

Hogrefe, C., S. S. Isukapalli, X. G. Tang, P. G. Georgopoulos, S. He, E. E. Zalewsky, W. Hao, J. Y. Ku, T. Key, and G. Sistla (2011), Impact of biogenic emission uncertainties on the simulated response of ozone and fine particulate matter to anthropogenic emission reductions, *J. Air Waste Man. Assoc.*, *61*(1), 92–108.

Horowitz, L. W., A. M. Fiore, G. P. Milly, R. C. Cohen, A. Perring, P. J. Wooldridge, P. G. Hess, L. K. Emmons, and J. F. Lamarque (2007), Observational constraints on the chemistry of isoprene nitrates over the eastern United States, *J. Geophys. Res.*, *112*, D12S08, doi:10.1029/2006JD007747.

Jacobs, M. I., W. J. Burke, and M. J. Elrod (2014), Kinetics of the reactions of isoprene-derived hydroxynitrates: Gas phase epoxide formation and solution phase hydrolysis, *Atmos. Chem. Phys.*, *14*, 8933–8946.

Jaeglé, L., L. Steinberger, R. V. Martin, and K. Chance (2005), Global partitioning of NO_x sources using satellite observations: Relative roles of fossil fuel combustion, biomass burning and soil emissions, *Faraday Disc.*, *130*, 407–423.

Jenkin, M. E., S. M. Saunders, and M. J. Pilling (1997), The tropospheric degradation of volatile organic compounds: A protocol for mechanism development, *Atmos. Env.*, *31*(1), 81–104.

Karl, T., P. Misztal, H. Jonsson, S. Shertz, A. Goldstein, and A. Guenther (2013), Airborne flux measurements of BVOCs above Californian Oak Forests: Experimental investigation of surface and entrainment fluxes, OH densities, and damkohler numbers, *J. Atmos. Sci.*, *70*(10), 3277–3287.

Knote, C., A. Hodzic, and J. L. Jimenez (2015), The effect of dry and wet deposition of condensable vapors on secondary organic aerosols concentrations over the continental US, *Atmos. Chem. Phys.*, *15*, 1–18.

Krol, M. C., M. J. Molemaker, and J. V. G. de Arellano (2000), Effects of turbulence and heterogeneous emissions on photochemically active species in the convective boundary layer, *J. Geophys. Res.*, *105*(D5), 6871–6884, doi:10.1029/1999JD900958.

LaFranchi, B. W., et al. (2009), Closing the peroxy acetyl nitrate budget: Observations of acyl peroxy nitrates (PAN, PPN, and MPAN) during BEARPEX 2007, *Atmos. Chem. Phys.*, *9*, 7623–7641.

Lenschow, D. H., R. Pearson, and B. B. Stankov (1981), Estimating the ozone budget in the boundary-layer by use of aircraft measurements of ozone eddy flux and mean concentration, *J. Geophys. Res.*, *86*(NC8), 7291–7297, doi:10.1029/JC086iC08p07291.

Li, X., et al. (2014), Missing gas-phase source of HONO inferred from zeppelin measurements in the troposphere, *Science*, *344*(6181), 292–296.

Magnani, F., et al. (2007), The human footprint in the carbon cycle of temperate and boreal forests, *Nature*, *447*(7146), 849–851.
Mao, J., et al. (2012), Insights into hydroxyl measurements and atmospheric oxidation in a California forest, *Atmos. Chem. Phys.*, *12*, 8009–8020.
McNeill, V. F., J. L. Woo, D. D. Kim, A. N. Schwier, N. J. Wannell, A. J. Sumner, and J. M. Barakat (2012), Aqueous-phase secondary organic aerosol and organosulfate formation in atmospheric aerosols: A modeling study, *Env. Sci. Technol.*, *46*(15), 8075–8081.
Millet, D. B., D. J. Jacob, K. F. Boersma, T. M. Fu, T. P. Kurosu, K. Chance, C. L. Heald, and A. Guenther (2008), Spatial distribution of isoprene emissions from North America derived from formaldehyde column measurements by the OMI satellite sensor, *J. Geophys. Res.*, *113*, D02307, doi:10.1029/2007JD008950.
Misztal, P. K., T. Karl, R. Weber, H. H. Jonsson, A. B. Guenther, and A. H. Goldstein (2014), Airborne flux measurements of biogenic volatile organic compounds over California, *Atmos. Chem. Phys.*, *14*, 10,631–10,647.
Nguyen, T. B., J. D. Crounse, A. P. Teng, J. M. S. Clair, F. Paulot, G. M. Wolfe, and P. O. Wennberg (2015), Rapid deposition of oxidized biogenic compounds to a temperate forest, *P. Nat. Acad. Sci. U.S.A.*, *112*(5), E392–E401.
Park, J. H., A. H. Goldstein, J. Timkovsky, S. Fares, R. Weber, J. Karlik, and R. Holzinger (2013), Active atmosphere-ecosystem exchange of the vast majority of detected volatile organic compounds, *Science*, *341*(6146), 643–647.
Paulot, F., J. D. Crounse, H. G. Kjaergaard, A. Kurten, J. M. St. Clair, J. H. Seinfeld, and P. O. Wennberg (2009), Unexpected epoxide formation in the gas-phase photooxidation of isoprene, *Science*, *325*(5941), 730–733.
Paulot, F., D. K. Henze, and P. O. Wennberg (2012), Impact of the isoprene photochemical cascade on tropical ozone, *Atmos. Chem. Phys.*, *12*, 1307–1325.
Peeters, J., T. L. Nguyen, and L. Vereecken (2009), HO_x radical regeneration in the oxidation of isoprene, *Phys. Chem. Chem. Phys.*, *11*(28), 5935–5939.
Peeters, J., J.-F. Muller, T. Stavrakou, and V. S. Nguyen (2014), Hydroxyl radical recycling in isoprene oxidation driven by hydrogen bonding and hydrogen tunneling: The upgraded LIM1 mechanism, *J. Phys. Chem. A*, *118*, 8625–8643.
Perring, A. E., et al. (2009), Airborne observations of total RONO2: New constraints on the yield and lifetime of isoprene nitrates, *Atmos. Chem. Phys.*, *9*(4), 1451–1463.
Rohrer, F., et al. (2014), Maximum efficiency in the hydroxyl-radical-based self-cleansing of the troposphere, *Nature Geosci.*, *7*, 559–563.
Saunders, S. M., M. E. Jenkin, R. G. Derwent, and M. J. Pilling (2003), Protocol for the development of the Master Chemical Mechanism, MCM v3 (part A): Tropospheric degradation of non-aromatic volatile organic compounds, *Atmos. Chem. Phys.*, *3*, 161–180.
Smith, M. L., A. K. Bertram, and S. T. Martin (2012), Deliquescence, efflorescence, and phase miscibility of mixed particles of ammonium sulfate and isoprene-derived secondary organic material, *Atmos. Chem. Phys.*, *12*(20), 9613–9628.
Stone, D., L. K. Whalley, and D. E. Heard (2012), Tropospheric OH and HO_2 radicals: Field measurements and model comparisons, *Chem. Soc. Rev.*, *41*, 6348–6404.
Unger, N., et al. (2013), Photosynthesis-dependent isoprene emission from leaf to planet in a global carbon-chemistry-climate model, *Atmos. Chem. Phys.*, *13*(20), 10,243–10,269.
Wang, Y. H., D. J. Jacob, and J. A. Logan (1998), Global simulation of tropospheric O-3-NO_x-hydrocarbon chemistry. 1. Model formulation, *J. Geophys. Res.*, *103*(D9), 10,713–10,725, doi:10.1029/98JD00158.
Warneke, C., et al. (2010), Biogenic emission measurement and inventories determination of biogenic emissions in the eastern United States and Texas and comparison with biogenic emission inventories, *J. Geophys. Res.*, *115*, D00F18, doi:10.1029/2009JD012445.
Wesely, M. L. (1989), Parameterization of surface resistances to gaseous dry deposition in regional-scale numerical models, *Atmos. Env.*, *23*(6), 1293–1304.
Wiedinmyer, C., et al. (2005), Ozarks Isoprene Experiment (OZIE): Measurements and modeling of the "isoprene volcano", *J. Geophys. Res.*, *110*, D18307, doi:10.1029/2005JD005800.
Wolfe, G. M., J. A. Thornton, R. L. N. Yatavelli, M. McKay, A. H. Goldstein, B. LaFranchi, K. E. Min, and R. C. Cohen (2009), Eddy covariance fluxes of acyl peroxy nitrates (PAN, PPN and MPAN) above a Ponderosa pine forest, *Atmos. Chem. Phys.*, *9*(2), 615–634.
Xu, L., et al. (2015), Effects of anthropogenic emissions on aerosol formation from isoprene and monoterpenes in the southeastern United States, *P. Nat. Acad. Sci. U.S.A.*, *112*(1), 37–42.